separations

MDPI

Article

Study on the Dewatering Mechanism of Fine Phosphate Tailings Slurrys Based on the Particle-Agent Interaction and Sedimentation Property

Fang Li [1,2], Yuping Fan [1], Yuanpeng Fu [1,3], Xiaomin Ma [1], Xianshu Dong [1,*], Yangge Zhu [3], Wei Xiao [1] and Wenjie Fang [1]

[1] School of Mining Engineering, Taiyuan University of Technology, Taiyuan 030024, China; lifang@xingfagroup.com (F.L.); 19880628fyp@163.com (Y.F.)
[2] Hubei Xingfa Chemical Group Co., Ltd., Yichang 443311, China
[3] State Key Laboratory of Mineral Processing, BGRIMM Technology Group, Beijing 100044, China
* Correspondence: dongxianshu@tyut.edu.cn

Abstract

Fluorapatite is a typical phosphate rock resource. Fluorapatite tends to generate fine mud agglomeration, which induces dehydration challenges owing to its inherently fine particle size and negative surface charge. In this paper, phosphate tailings slurries from a phosphate mine in Hubei Province, China, were selected as the research object, and flocculation–dehydration experiments were conducted using anionic, cationic, and nonionic polyacrylamide (PAM) flocculants. The results show that the maximum settling velocity is 51 mm/s and the moisture content of filter cake is 41.54%, which were obtained when the unit consumption of cationic flocculant with molecular weight 12 million was 1000 g/t. The mechanism of sedimentation and dehydration was studied by infrared spectroscopy and a particle size analyzer. The results showed that polyacrylamide was effectively adsorbed on the mineral surface, and the size of flocs increased significantly. Finally, the mechanism of sedimentation and dehydration was proposed. It has important guiding significance for the efficient solid–liquid separation and water circulation of fluorapatite mineral processing wastewater.

Keywords: fluorapatite; polyacrylamide; flocculation; dehydration; process mechanism; solid–liquid separation

Check for updates

Academic Editor: Jian Liu

Received: 8 March 2026
Revised: 1 April 2026
Accepted: 8 April 2026
Published: 15 April 2026

Copyright: © 2026 by the authors. Licensee MDPI, Basel, Switzerland. This article is an open access article distributed under the terms and conditions of the Creative Commons Attribution (CC BY) license.

1. Introduction

Phosphate ore is a strategic mineral in China. China boasts abundant phosphate ore reserves, ranking second worldwide in phosphate resource reserves. However, few high-grade ores can be directly utilized, with the majority being low-grade collophane ore [1–4]. The high impurity content considerably complicates the beneficiation process, driving up capital expenditure and the final production cost of commercial phosphate rock [5,6]. From the perspectives of sustainable development, improving resource utilization efficiency, reducing environmental pollution, and minimizing ecological damage, conducting research on the efficient utilization of low-grade phosphorus resources is urgent. However, there are many technical issues with its beneficiation process, including the settling of concentrate and tailings [7–9]. To achieve good selection results, phosphate ore usually has high requirements for grinding fineness. However, as the grinding particle size decreases, the settling of concentrates and tailings becomes increasingly difficult. Usually, it is necessary

to increase production capacity by adding thickening equipment or adding flocculants to achieve more efficient sedimentation [10–12].

At present, the reagents used for flocculation and sedimentation of phosphate tailings are mainly divided into three categories: inorganic flocculant, natural organic flocculant and synthetic organic flocculant. Inorganic flocculants, such as polyaluminum chloride and polyferric sulfate, have been used in early stages because of their low price and strong charge neutralization ability. However, they have some defects, such as high dosage, loose and fragile flocs, and poor dewatering performance, and they are easily influenced by pulp pH and ion composition [13,14], so their application effect in fine-grained phosphate tailings with a complex ion system is limited. Natural organic flocculants, including chitosan, xanthan gum and flax seed-derived bioflocculants, are environmentally friendly and biodegradable. Some studies have confirmed that they can achieve a certain particle bridging effect in the flocculation of phosphate tailings [15–17], but these agents have some problems such as high preparation cost, low flocculation efficiency and poor adaptability to acidic pulp, which makes it difficult to meet the needs of industrial production for high efficiency and low cost.

Synthesis of organic flocculants is the core direction of research and application of phosphate tailings flocculation at present, among which a polyacrylamide (PAM) series has become a research hotspot because of its controllable molecular chain, rich charge types and strong bridging ability. According to the charge characteristics, PAM can be divided into three types: cationic (CPAM), anionic (APAM) and nonionic (NPAM). Different types of PAM with different molecular weights show significant differences in the flocculation of phosphate tailings: NPAM relies on molecular chain bridging to achieve particle aggregation but lacks the ability of charge neutralization, and its flocculation efficiency is low in strongly negative phosphate tailings [18–22]; APAM can be bridged by complexing anionic groups with metal ions in pulp, but its effect is easily affected by interfering ions such as phosphate. CPAM can neutralize the negative charges on the surface of tailings particles by electrostatic charge, which destroys its colloidal stability. At the same time, CPAM can bridge the particles efficiently with the help of long molecular chains, showing more excellent effects in the flocculation of phosphate tailings. The existing research has confirmed the feasibility of PAM series reagents in the flocculation of phosphate rock tailings, but most of the research focuses on the conventional phosphate rock tailings system. The research on the compatibility and action mechanism of reagents in the complex ionic environment of fine-grained phosphate tailings slurries is still insufficient, and there is no systematic comparison of molecular weight, dosage and flocculation effect of different types of PAM; the optimal PAM reagent system for fine-grained phosphate tailings slurries has not been clarified.

This paper selected phosphate tailings from a mine in Yichang for experimental research. Due to the fine particles and high mud content of the phosphate tailings, flocculation and sedimentation tests were conducted using organic flocculants of different ion types and molecular weights. This research explored the influence of organic flocculants on the flocculation and sedimentation behavior of the phosphate ore. First of all, the polyacrylamide (PAM) flocculant used in this paper is a very conventional chemical in the field of phosphate ore tailings dehydration, which constitutes the practical basis for the experiments designed in this study. Specifically, the interaction between flocculant molecules and mineral surfaces, the adsorption characteristics, and the bridging behavior of macromolecular flocculants were investigated. This study reveals the impact mechanism of these flocculants on sedimentation, providing theoretical support and technical reference for the further development of phosphate tailings thickening and dewatering technology.

2. Materials and Methods

2.1. Materials and Reagents

The phosphorus flotation tailings slurry was collected from a phosphate ore plant in Yichang City, Hubei Province. In this study, it is hereinafter referred to simply as phosphate tailings slurry. The basic properties of the slurry are shown in the following figures and tables. Figure 1 displays the XRD diffraction pattern of the phosphate tailings slurry, and Table 1 presents the XRF analysis results. Figure 2 illustrates the laser particle size analysis of the phosphate tailings slurry, and Figure 3 shows the process mineralogy analysis results. Based on the XRD characteristic peaks and XRF results, the main gangue minerals in the phosphate tailings slurry are dolomite ($CaMg(CO_3)_2$) and gypsum ($CaSO_4 \cdot 2H_2O$), with high contents of CaO and MgO, along with some fluorapatite and other minerals. Ca^{2+} and Mg^{2+} ions released from dolomite and gypsum directly alter the pulp water quality, thereby impairing the sedimentation performance of the phosphate tailings slurry. The results of water quality analysis showed that the phosphate slurry had a pH of 3.19, an electrical conductivity of 12.98 mS/m, and a Zeta potential of −5.307 mV. Additionally, the residual concentrations of the amine collector and flocculant in the supernatant were 0.46 g/L and 3.83 g/L, respectively. Residual organic agents will cause difficulties in the subsequent dewatering and settlement of tailings.

Particle size analysis (Figure 2) reveals a relatively narrow particle size distribution for the phosphate tailings slurry, with a D90 of 18.664 μm and a D50 of 3.700 μm. Fine-grained minerals are predominant by a significant margin over coarse-grained ones, classifying this slurry as a fine-grained phosphate tailings system.

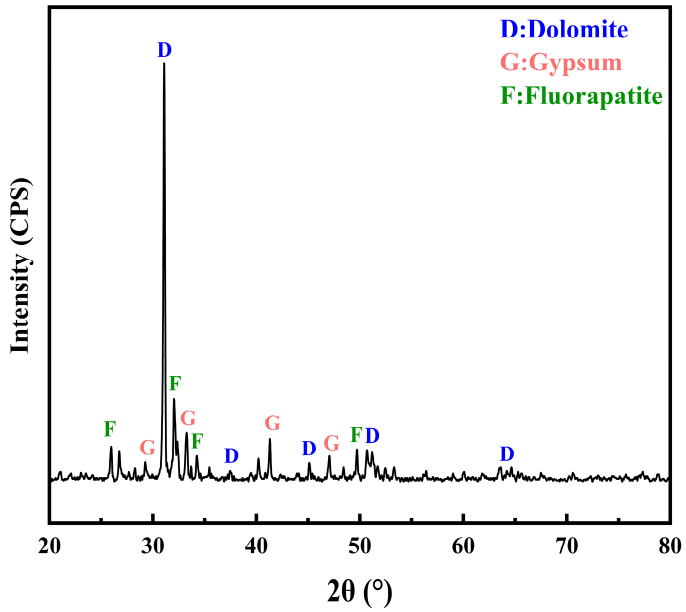


Figure 1. XRD analysis of phosphorus tailings slurry.

Table 1. The chemical compositions of phosphorus tailings slurry.

Mineral	Content (wt.%)										
Phosphate ore pulp	CaO	MgO	SiO_2	A_2O_3	Fe_2O_3	P_2O_5	SO_3	F	K_2O	CO_2	Other
	32.78	15.73	6.82	5.12	1.41	4.89	0.12	0.32	0.21	32.32	0.28

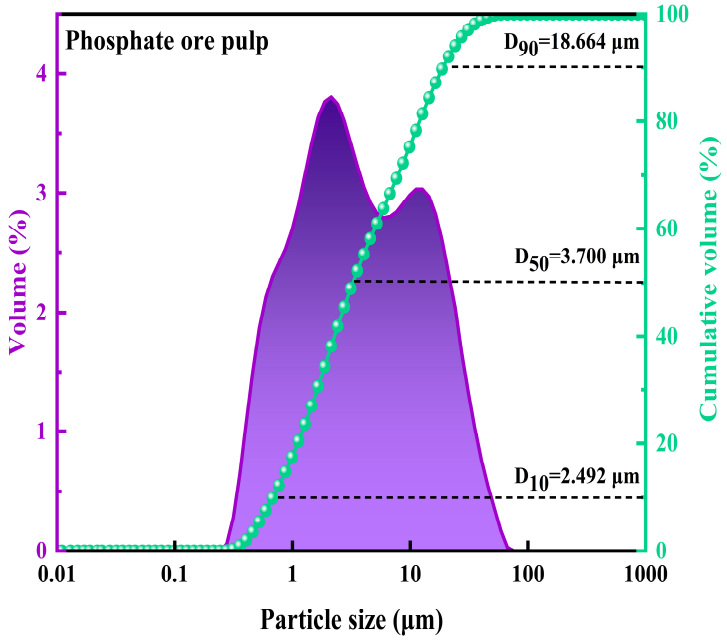


Figure 2. Particle size composition analysis of phosphorus tailings slurry.

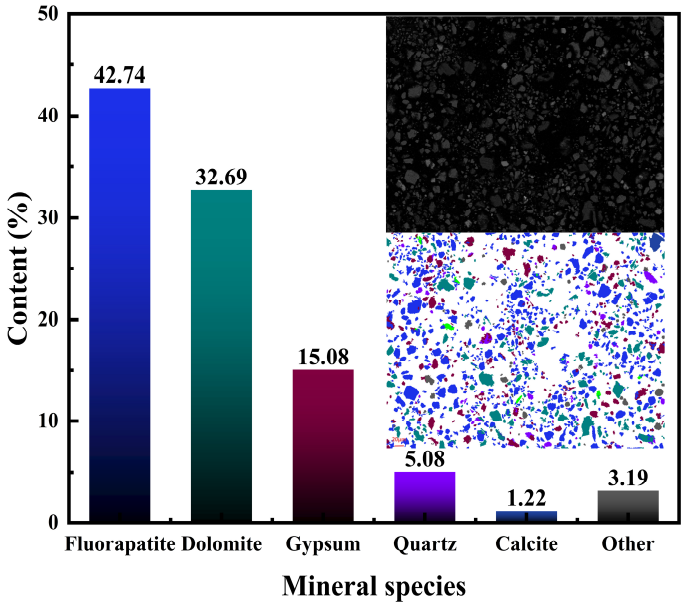


Figure 3. Process mineralogy analysis results of phosphorus tailings slurry.

The process mineralogy analysis results in Figure 3 reveal that fluorapatite, dolomite, gypsum, and quartz are the main mineral components of the phosphate tailings slurry. Among them, fluorapatite accounts for 42.74%, while dolomite and gypsum account for 32.69% and 15.08%, respectively, which is generally consistent with the XRD and XRF analysis results. In the phosphate tailings slurry, compared to fluorapatite, dolomite and gypsum exhibit more complete monomer liberation. Their strong hydrophilicity is the primary reason for the challenging sedimentation of the phosphate tailings slurry.

The chemical reagents used in this study are as follows: CPAM (Mw: 6 million; 12 million; Charge density: 2.76 mmol/g), APAM (Mw: 6 million; 12 million; Charge density: 2.49 mmol/g), and NPAM (Mw: 6 million; 12 million; Charge density: 0.22 mmol/g), all serving as flocculants. The reagents were sourced from Shanghai Aladdin Biochemical Technology Co., Ltd. (Shanghai, China). HCl and NaOH were used as pH adjusters, and KCl (Shanghai Aladdin Biochemical Technology Co., Ltd., Shanghai, China) was employed

for Zeta potential measurements. All reagents were of analytical grade, and deionized water (resistivity = 18.25 MΩ·cm) was used throughout the experiments.

2.2. Pulp Flocculation Sedimentation Test

The flocculants used in the experiment are mainly NPAM, CPAM, and APAM with molecular weights of 6 million and 12 million. The core differences between non-ionic polyacrylamide (NPAM), cationic polyacrylamide (CPAM), and anionic polyacrylamide (APAM) are as follows: First of all, NPAM has no charged functional groups on its molecular chain, relying on amide groups for hydrophilicity; CPAM contains cationic functional groups such as quaternary ammonium salts (ionicity: 30–50% in this experiment) and is positively charged overall; and APAM has anionic functional groups such as carboxyl/sulfonic acid groups (hydrolysis degree: 20–30% in this experiment) and is negatively charged in aqueous solutions. Secondly, NPAM mainly relies on the "bridging effect" to connect particles via molecular chains; CPAM combines "charge neutralization + bridging"—its positive charges neutralize the negative charges on tailings particles before aggregation; and APAM achieves flocculation through "electrostatic repulsion regulation + bridging", stretching molecular chains to capture fine particles. So, NPAM is suitable for neutral water and particles with weak charges, featuring strong stability but moderate efficiency; CPAM is well-adapted to phosphate tailings slurries (negatively charged), offering high dehydration efficiency and low filter cake moisture content, and is widely used in phosphate ore dehydration; and APAM is suitable for fine-particle systems but is prone to interference from calcium and magnesium ions in ore pulp.

After thoroughly stirring the phosphate slurry with a mixer, 250 mL of the slurry was transferred into a large-stoppered measuring cylinder. We weighed an appropriate amount of PAM to prepare a 0.1% flocculant solution. The required dosage of flocculant solution (500, 625, 750, 875, 1000, and 1125 $g \cdot t^{-1}$) was extracted using a syringe and added to the measuring cylinder containing the phosphate slurry. To ensure thorough mixing of the flocculant and slurry, the measuring cylinder was immediately inverted rapidly 10 times. The measuring cylinder was placed on the table to begin the settling experiment and a stopwatch was used to time it, recording the corresponding scale values of the clear layer liquid level at different times. After settling for 5 min, we recorded the corresponding scale values of the sediment layer and took a small amount of supernatant with a pipette. The transmittance and absorbance of the supernatant were determined using a spectrophotometer. Each group of experiments was repeated three times. After the experiment, the average value of each parameter of each group of experiments was taken to calculate the pulp settling speed. The specific formula is as follows:

$$V = \frac{M\sum_{i=A}^{B} T_i H_i - \left(\sum_{i=A}^{B} T_i\right)\left(\sum_{i=A}^{B} H_i\right)}{M\sum_{i=A}^{B} T_i^2 - \left(\sum_{i=A}^{B} T_i\right)^2} \times 6$$

V—clarifies the initial settling velocity of the interface, mm/s;
T_i—a certain cumulative moment, s;
H_i—corresponding to the cumulative descent distance of Ti clarification interface, mm;
A, B—select the starting and ending points for calculating settlement velocity, respectively;
M—accumulated number of points from A to B (M−B−A + 1).

2.3. ICP-OES Measurements

The elemental concentration analysis in the slurry was conducted using an Agilent 7800 MS instrument (Agilent, Santa Clara, CA, USA). For each test, 2 g of phosphate tailings slurry was mixed with 100 mL of deionized water and stirred mechanically until

homogeneous. After allowing the mixture to stand for 5 min, the supernatant from both the sample without PAM and the sample with PAM was collected separately for centrifugation. Following centrifugation, the supernatant was taken for ICP-OES measurement.

2.4. Particle Size Testing

The particle size distribution of the slurry was tested using a Malvern Mastersizer 3000 (Malvern Panalytical, Malvern, UK). The phosphate tailings slurry was first filtered using a vacuum filter and then dried in an oven. A small amount of the dried sample was placed in a beaker containing deionized water. The beaker was then positioned on the dispersion unit stage of the laser particle size analyzer. The particle size of the sample was analyzed by measuring the diffraction pattern generated when the laser beam within the instrument irradiates the sample particles.

2.5. Floc Morphology Testing

The morphology of phosphorus tailings slurry particles and flocs was observed and captured using a Nikon SMZ745T (Nikon Corporation, Tokyo, Japan) stereomicroscope. Following the procedure described in the sedimentation test above, flocs from the compression layer were gently extracted with a specialized rubber-tip dropper (5 mm in diameter) and placed on a custom-made stage. The sample was then diluted with water to ensure uniform dispersion of the flocs. The morphology of slime flocs under different conditions was observed and photographed under 10× and 20× objective lenses. For each reagent condition, multiple samples were collected and photographed, with over 10 floc images (containing no fewer than 80 flocs) obtained to ensure data representativeness.

2.6. Dynamic Characterization Test of Particle Size

The dynamic distribution of particle floc size was measured using a Particle Video Microscope EasyViewer 100 (Mettler Toledo, Greifensee, Switzerland). For each measurement, samples before and after reagent treatment were separately mixed and stirred with deionized water. The stirring speed was initially set at 800 r/min for 2 min to ensure thorough dispersion of the slurry and then adjusted to 300 r/min to promote the formation of floc aggregates. Continuous monitoring was performed for 15 min under constant stirring. Throughout the monitoring process, the PVM probe remained fully immersed in the slurry solution.

2.7. Zeta Potential Testing

The surface potential of minerals was measured using a Malvern Zetasizer Nano ZS90 (Malvern Instrument, Malvern, UK). For each test, 20 mg of the sample was first mixed with 50 mL of KCl solution (1×10^{-3} mol/L) in a beaker and stirred for 2 min. The pH of the slurry was then adjusted within the range of 4–10. Corresponding reagents were added according to the experimental conditions, followed by stirring and a 15 min settling period. The supernatant in the beaker was subsequently removed for Zeta potential measurement. Each experimental condition was tested three times, and the average of the results was taken as the final value.

2.8. FTIR Testing

Infrared spectroscopy of the reagents and phosphate ore samples was performed using a Thermo Scientific Nicolet iS50 FTIR spectrometer (Thermo Fisher Scientific, Waltham, MA, USA). A 2 g ground phosphate ore sample was mixed with 60 mL of deionized water in a beaker and stirred for 2 min. Corresponding reagents were then added according to the experimental conditions, followed by additional stirring. The mixture was subsequently filtered and dried (in a constant-temperature vacuum dryer at 25 °C). The dried

powder sample was mixed with pure KBr at a ratio of 1:100, and a pellet was prepared using a hydraulic press. Infrared spectra were obtained in transmission mode, covering a wavenumber range of 4000–400 cm^{-1} with a resolution of 2 cm^{-1}.

3. Results and Discussion

3.1. Analysis of Complex Components of Pulp

Based on the analysis results of XRD, XRF, and process mineralogy of the samples, the main minerals in the phosphate tailings slurry are dolomite, gypsum, and fluorapatite. The dissolved metal ions from partial dissolution on the surfaces of these minerals directly influence the chemical properties of the ore slurry. Figures 4–6 present the solution chemistry analysis results of ions dissolved from dolomite, gypsum, and fluorapatite in the ore slurry, respectively. The initial ion concentration is set to 0.1 mol/L. Since the content of F element in fluorapatite is relatively low, apatite was used to simplify the solution chemistry calculation process. Figure 6 shows the slurry potential of the three minerals under different pH conditions.

Chemical reaction and equilibrium constant of dolomite dissolution ions [23]:

$$CaMg(CO_3)_2 \rightleftharpoons Ca^{2+} + Mg^{2+} + 2CO_3^{2-} \quad pK = 19.35 \tag{1}$$

$$Ca^{2+} + HCO_3^- \rightleftharpoons CaHCO_3^+ \quad pK = -0.87 \tag{2}$$

$$CaHCO_3^+ \rightleftharpoons H^+ + CaCO_{3(aq)} \quad pK = 7.99 \tag{3}$$

$$Ca^{2+} + (OH)^- \rightleftharpoons Ca(OH)^+ \quad pK = -1.30 \tag{4}$$

$$Ca(OH)^+ + (OH)^- \rightleftharpoons Ca(OH)_{2(s)} \quad pK = 1.30 \tag{5}$$

$$Ca(OH)_{2(aq)} \rightleftharpoons Ca(OH)_{2(s)} \quad pK = -5.10 \tag{6}$$

$$Mg^{2+} + HCO_3^- \rightleftharpoons MgHCO_3^+ \quad pK = -1.16 \tag{7}$$

$$MgHCO_3^+ \rightleftharpoons H^+ + MgCO_{3(aq)} \quad pK = 8.09 \tag{8}$$

$$Mg^{2+} + (OH)^- \rightleftharpoons Mg(OH)^+ \quad pK = -2.57 \tag{9}$$

$$Mg(OH)^+ + (OH)^- \rightleftharpoons Mg(OH)_{2(s)} \quad pK = -8.48 \tag{10}$$

$$Mg(OH)_{2(aq)} \rightleftharpoons Mg(OH)_{2(s)} \quad pK = -2.67 \tag{11}$$

$$CO_3^{2-} + H_2O \rightleftharpoons HCO_3^- + OH^- \quad pK = 3.67 \tag{12}$$

$$HCO_3^- + H_2O \rightleftharpoons H_2CO_3 + OH^- \quad pK = 7.62 \tag{13}$$

Dolomite ($CaMg(CO_3)_2$) is a typical carbonate mineral, and carbonate minerals generally exhibit high solubility. Ca^{2+}, Mg^{2+}, and CO_3^{2-} in dolomite continuously dissolve

into the ore slurry. As shown in Figure 5, the concentrations of CO_3^{2-}, HCO_3^-, $CaOH^+$, $CaHCO_3^+$ and $MgOH^+$ all increase with the rise in pH from 2 to 7 under acidic conditions, while the concentration of $MgHCO_3^+$ decreases. Ca^{2+} reacts with OH^- generated by the hydrolysis of CO_3^{2-} in the solution to form a significant amount of CaOH(s) [24], which leads to a decrease in the positive charge components in the ore slurry. The pH of the phosphate tailings slurry used in this experiment is 3.19, which corresponds to a Zeta potential of −8.07 mV for the dolomite slurry, as shown in Figure 6.

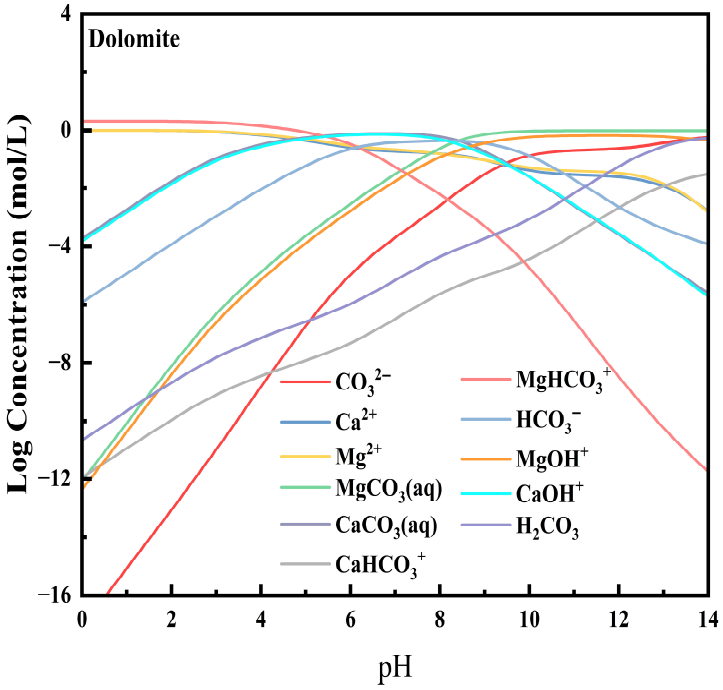


Figure 4. Solution chemical analysis of pulp.

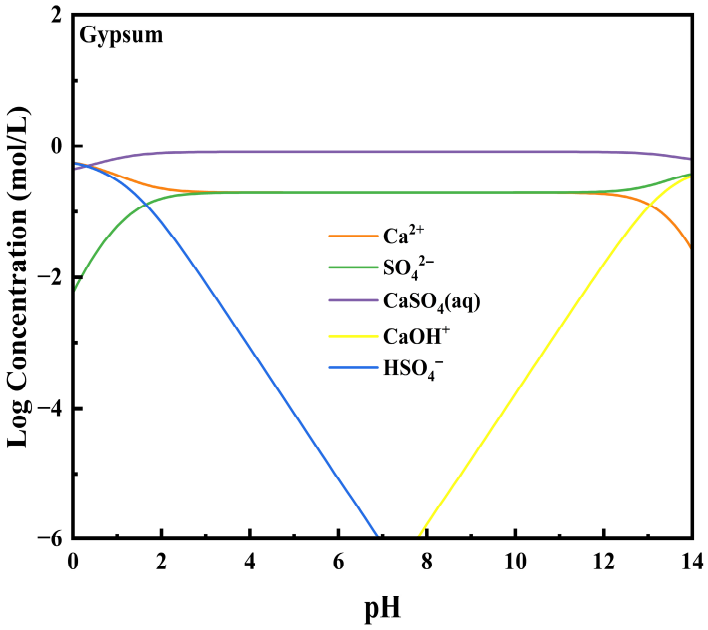


Figure 5. Solution chemical analysis of gypsum.

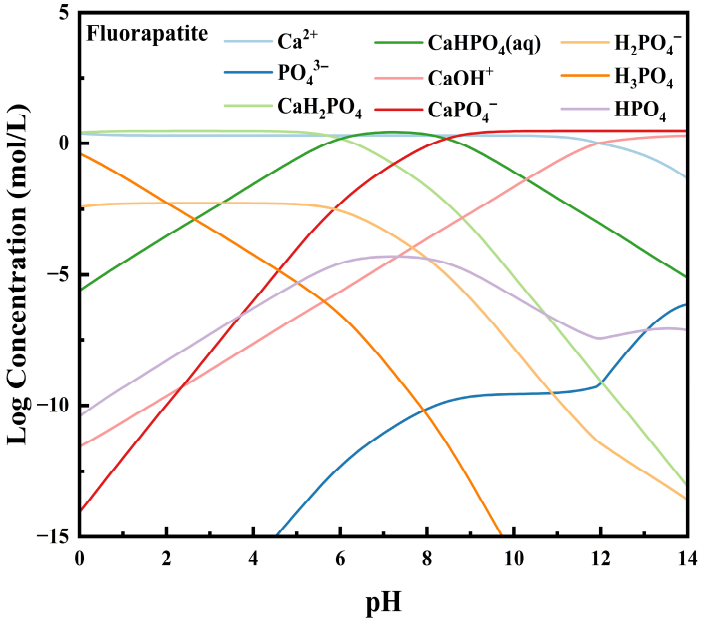


Figure 6. Solution chemical analysis of fluorapatite.

Chemical reaction and equilibrium constant of gypsum dissolution ions [25]:

$$CaSO_{4(aq)} \rightleftharpoons Ca^{2+} + SO_4^{2-} \quad pK = 4.61 \tag{14}$$

$$Ca^{2+} + OH^- \rightleftharpoons CaOH^+ \quad pK = -1.40 \tag{15}$$

$$Ca^{2+} + 2OH^- \rightleftharpoons Ca(OH)_{2(aq)} \quad pK = -2.77 \tag{16}$$

$$H^+ + SO_4^{2-} \rightleftharpoons HSO_4^- \quad pK = -1.92 \tag{17}$$

In the dissolved ion components of gypsum ($CaSO_4 \cdot 2H_2O$), the pH increases of Ca^{2+}, SO_4^{2-}, and $CaSO_4$(aq) remain basically stable. As the pH increases, the concentration of HSO_4^- gradually decreases, while the concentration of $CaOH^+$ increases gradually. When the pH is 3.19, HSO_4^- is still the dominant component in the ore slurry, and the Zeta potential of the gypsum ore slurry is −2.39 mV at this pH.

Chemical reaction and equilibrium constant of fluorapatite dissolved ions [26]:

$$Ca_{10}(PO_4)_6(OH)_2 \rightleftharpoons 10Ca^{2+} + 6PO_4^{3-} + 2OH^- \quad pK = -115.00 \tag{18}$$

$$Ca^{2+} + HPO_4^{2-} \rightleftharpoons CaHPO_{4(aq)} \quad pK = 2.70 \tag{19}$$

$$H^+ + PO_4^{3-} \rightleftharpoons HPO_4^{2-} \quad pK = 2.70 \tag{20}$$

$$H^+ + HPO_4^{2-} \rightleftharpoons H_2PO_4^- \quad pK = 7.20 \tag{21}$$

$$H^+ + H_2PO_4^- \rightleftharpoons H_3PO_4 \quad pK = 2.15 \tag{22}$$

$$Ca^{2+} + H_2PO_4^- \rightleftharpoons CaH_2PO_4^+ \quad pK = 1.10 \tag{23}$$

$$Ca^{2+} + PO_4^{3-} \rightleftharpoons CaPO_4^- \quad pK = 6.46 \tag{24}$$

$$Ca^{2+} + HPO_4^{2-} \rightleftharpoons CaHPO_{4(aq)} \quad pK = 2.70 \tag{25}$$

$$CaHPO_{4(aq)} \rightleftharpoons CaHPO_{4(s)} \quad pK = 4.30 \tag{26}$$

As shown in Figure 7, with the increase in pH, the concentrations of H_3PO_4, $H_2PO_4^-$, and $CaH_2PO_4^+$ in the solution components of fluorapatite ($Ca_5[PO_4]_3F$) gradually decrease, while the concentrations of $CaOH^+$ and PO_4^{3-} gradually increase. At a pH of 3.19, the primary solution components in the fluorapatite ore slurry are Ca^{2+}, $H_2PO_4^-$, H_3PO_4, $CaPO_4^-$, and HPO_4^{2-}, among others. These components determine that the Zeta potential of the fluorapatite ore slurry tends to be negative, which is −10.21 mV.

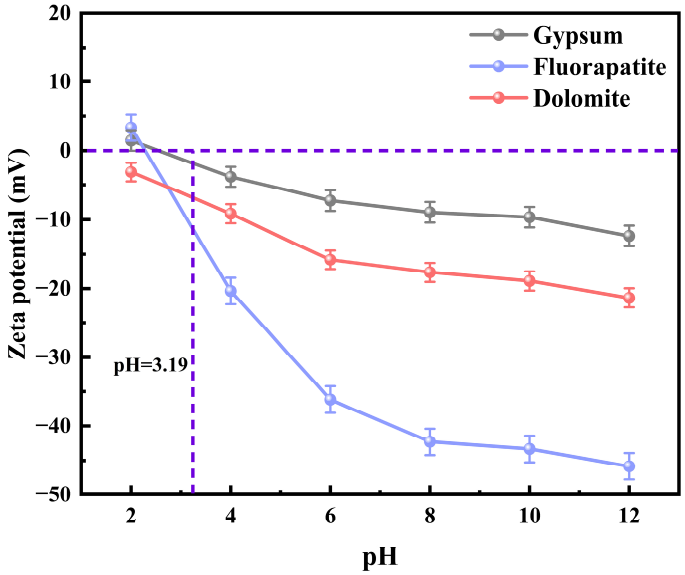


Figure 7. Pulp potentials of three minerals under different pH conditions.

Combined with the chemical analysis results of three mineral solutions, it can be seen that dolomite, gypsum and fluorapatite in phosphate ore pulp are mainly negative components, and the whole solution demonstrates negative potential. It is inferred that cationic flocculant has a good effect and can be effectively adsorbed on the surface of fine-grained minerals at this time. With the increase in pH, the mineral hydroxylation reaction is serious, and the pulp potential tends to be more negative.

3.2. Experimental Analysis of Pulp Flocculation and Sedimentation

In a beaker, prepare solutions of different types of flocculants with a mass fraction of 0.1%. Using a syringe, add the reagents to the phosphate tailings slurry according to the flocculant dosage standards of 500 g/t, 625 g/t, 750 g/t, 875 g/t, 1000 g/t, and 1125 g/t. Record the demarcation line values of solid–liquid separation at different time points, and plot sedimentation velocity graphs for different types of flocculants for comparative analysis.

Figure 8 shows the sedimentation characteristic curves of different types of polyacrylamide. Comparing the sedimentation velocities of flocculants with different molecular weights of the same reagent, it can be observed that flocculants with higher molecular weights within the same type have higher maximum sedimentation velocities than those with lower molecular weights. As the reagent dosage increases, all three types of polyacrylamide exhibit a trend of sedimentation velocity initially increasing and then stabilizing.

High reagent dosages do not significantly improve sedimentation velocity. Among them, CPAM shows a noticeable improvement in sedimentation velocity only after the dosage reaches 1000 g/t.

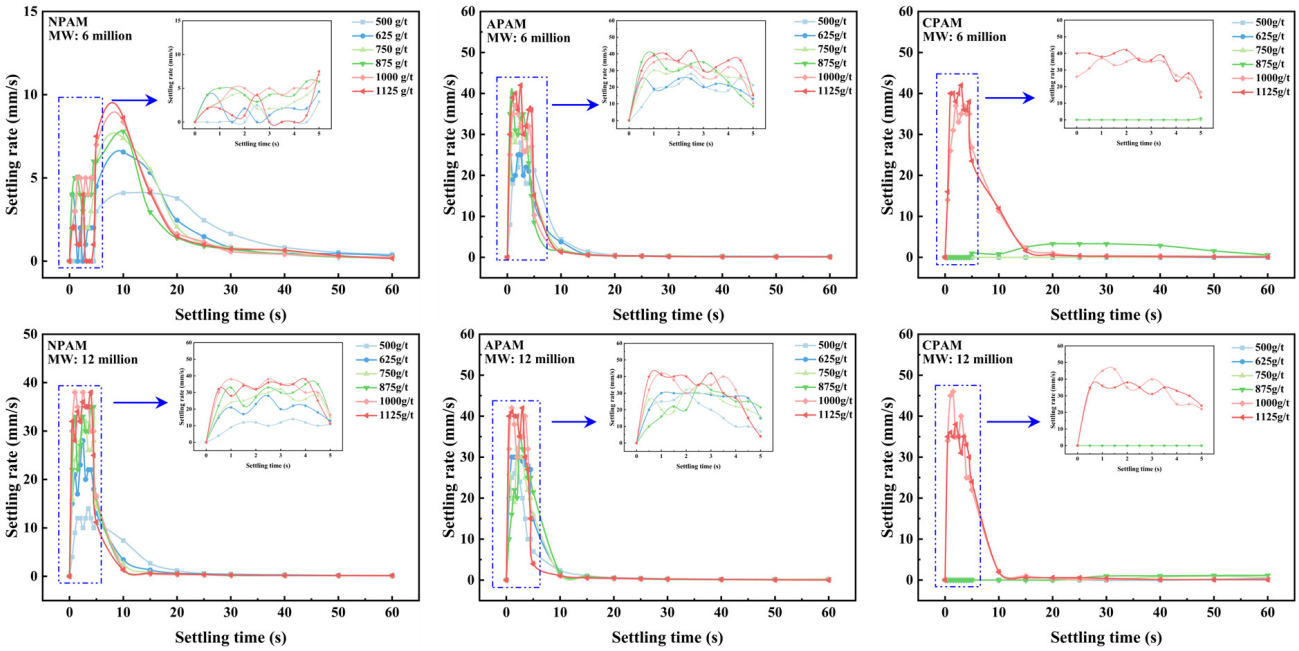


Figure 8. Analysis of sedimentation characteristics of phosphorus tailings pulp under different types of flocculants. (The inset represents the sedimentation rate in the first 5 s).

The superior sedimentation performance of CPAM and APAM compared with NPAM can be ascribed to their appropriate charge densities: CPAM possesses a charge density of 2.76 mmol/g, APAM has a charge density of 2.49 mmol/g, while NPAM is nearly charge-neutral with a charge density 0.22 mmol/g. The charged groups on CPAM and APAM enhance electrostatic interactions with phosphate ore particles, which promotes polymer adsorption and interparticle bridging, thereby leading to higher sedimentation velocities than NPAM.

Comparing the sedimentation velocities of different types of flocculants, the sedimentation velocities using CPAM and APAM are generally higher than those using NPAM. NPAM (MW: 12 million) reaches a peak sedimentation velocity of 38.0 mm/s at a dosage of 1000 g/t; APAM (MW: 12 million) reaches a peak sedimentation velocity of 42.0 mm/s at a dosage of 1125 g/t; and CPAM exhibits a relatively low initial sedimentation velocity at lower dosages. However, when CPAM (MW: 12 million) reaches a dosage of 1000 g/t, the initial sedimentation velocity increases rapidly, reaching a maximum of 51 mm/s. Additionally, the addition of CPAM results in a lower compressed layer of flocs and better compaction effects. Based on the comprehensive results of the flocculation–sedimentation experiments, CPAM (MW: 12 million) at a dosage of 1000 g/t is identified as the optimal reagent for the flocculation–sedimentation of fine-grained phosphate tailings slurry.

Figure 9 shows the absorbance values of various polyacrylamide types at different dosages. Absorbance measurements were performed using a spectrophotometer under test conditions simulating the scattering and absorption of incident light at 650 nm wavelength by phosphate ore following flocculant addition. As shown in the figure, the absorbance values of all six polyacrylamide types gradually decrease with increasing dosage. This indicates that higher concentrations of polyacrylamide yield superior flocculation and sedimentation effects. Comparing the absorbance values of different polyacrylamide types, NPAM exhibited the highest absorbance after treatment of the phosphate tailings slurry,

followed by APAM, while CPAM showed the lowest absorbance. At a dosage of 1000 g/t, both CPAM (MW: 6 million) and CPAM (MW: 12 million) exhibited absorbance values below 0.08, resulting in a generally clear supernatant. Based on the absorbance tests of different polyacrylamide types, CPAM (MW: 12 million) is the most suitable for flocculation and sedimentation of fine-grained phosphate tailings slurry, with a dosage of 1000 g/t. Above all, CPAM (MW: 12 million) at a dosage of 1000 g/t is the optimal combination under our experimental design among the tested chemicals.

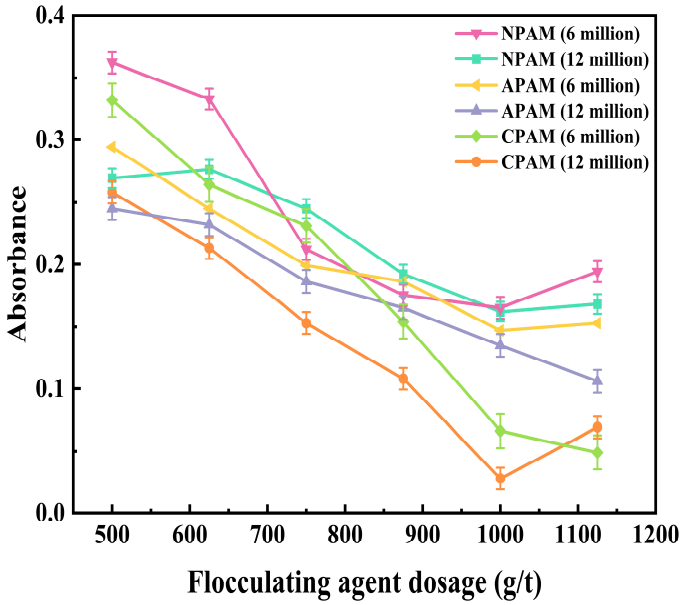


Figure 9. Supernatant absorbance of different types of flocculants.

3.3. ICP-OES Analyses

Based on the results of flocculation–sedimentation tests and absorbance measurements of flocculants, CPAM (MW: 12 million) was selected as the flocculant. The relative concentrations of unavoidable ions in the supernatant of the pulp before and after reagent addition were investigated using ICP-OES, as shown in Figure 10. Analysis of the unavoidable ion concentrations in the supernatant of the original pulp revealed that the slurry components of the phosphate ore were complex. The original pulp contains high concentrations of Ca^{2+} (769.21 mg/L), Mg^{2+} (1475.89 mg/L) and PO_4^{3-} (3022.77 mg/L) released by the dissolution of dolomite and gypsum. After adding 1000 g/t CPAM (MW: 12 million), the concentrations of these ions decreased significantly, with the PO_4^{3-} concentration dropping by 2672.8 mg/L (the most obvious decline). We further interpret this phenomenon: the cationic functional groups of CPAM can first form stable complexes with PO_4^{3-} through electrostatic interaction, which effectively reduces the competitive adsorption of PO_4^{3-} on the mineral surface and eliminates its interference with the bridging effect of CPAM molecules. Meanwhile, the chelation of CPAM with Ca^{2+} and Mg^{2+} can reduce the hydration film thickness of mineral particles, which is conducive to the close contact between particles and the full play of polymer bridging effect. These results indicate that CPAM (MW: 12 million) preferentially mitigates the adverse effects of phosphate groups in the pulp and subsequently further facilitates the flocculation and bridging of various unavoidable metal ions.

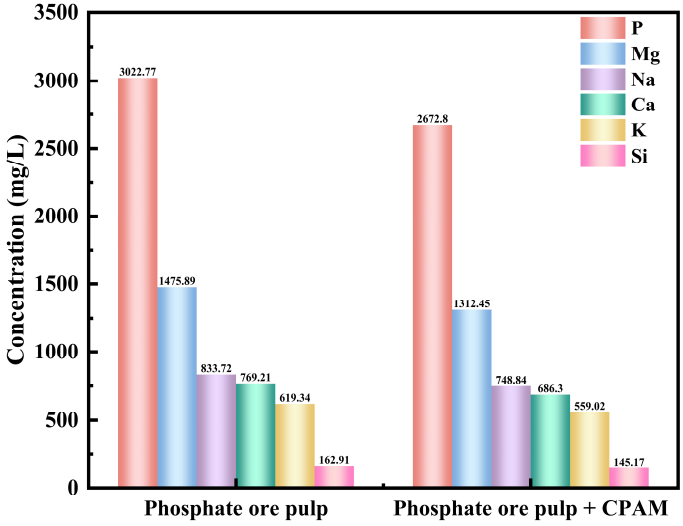


Figure 10. Concentration distribution of main unavoidable ions in the supernatant of phosphate tailings slurries before and after adding 1000 g/t CPAM (MW: 12 million).

3.4. Laser Particle Size Analysis and Floc Morphology Analysis

Based on the results of flocculation sedimentation tests, CPAM (MW: 12 million) was selected for particle size distribution and floc morphology analysis of the phosphate tailings slurry before and after reagent addition, as shown in Figures 11 and 12, with a dosage of 1000 g/t. As shown in Figure 11, before adding CPAM, the D90 of the phosphate tailings slurry was 17.572 μm and the D50 was 4.583 μm. The slurry contained a high proportion of fine particles, which were low in density and dispersed, leading to difficulties in sedimentation. After adding CPAM, the D90 of the phosphate tailings slurry increased to 71.473 μm and the D50 to 9.884 μm. A large number of slurry particles aggregated, forming flocs with larger particle sizes, which promoted the sedimentation of the phosphate tailings slurry. This verifies the advantage of CPAM (MW: 12 million) in the flocculation sedimentation process of fine-particle phosphate tailings slurry.

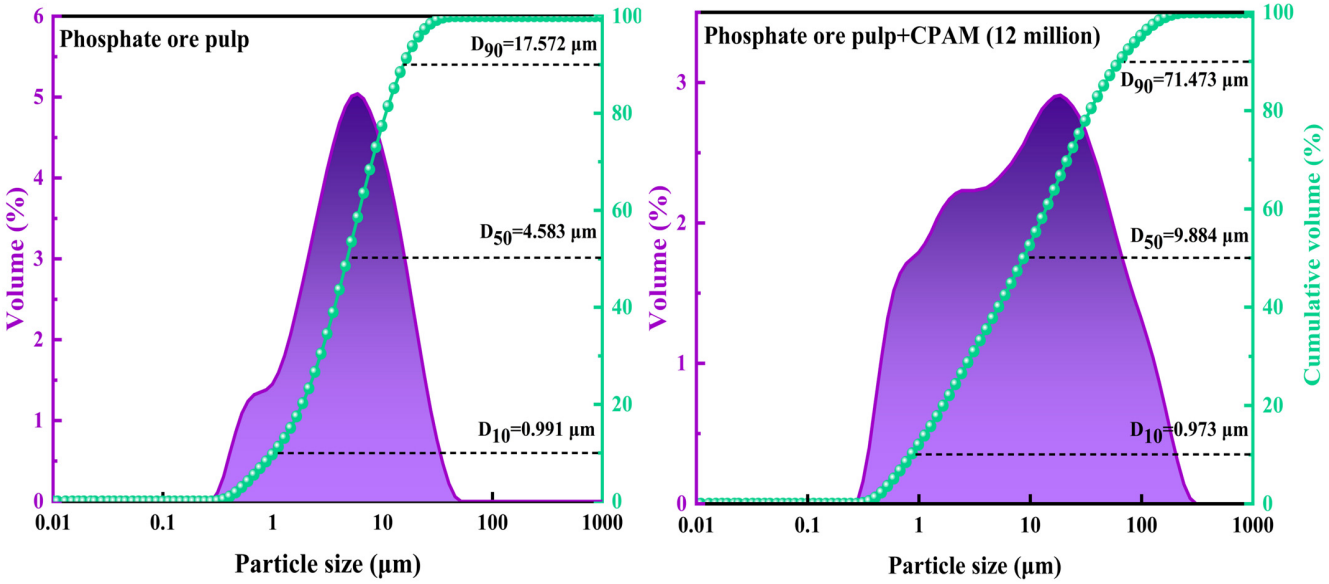


Figure 11. Laser particle size analysis of phosphate tailings slurries slurry before and after adding 1000 g/t CPAM (MW: 12 million).

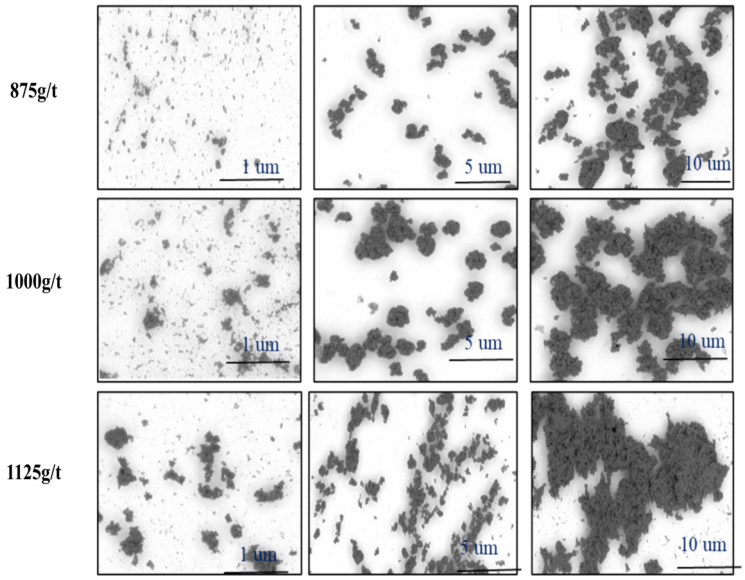


Figure 12. Floc morphology of phosphate tailings slurries slurry under an optical microscope (10×) treated with CPAM (MW: 12 million) at dosages of 875 g/t, 1000 g/t and 1125 g/t.

Floc morphology provides a more intuitive reflection of the effect of CPAM on phosphate ore particles. CPAM (MW: 12 million), which exhibited excellent sedimentation performance, was selected, and microscope images of flocs were captured at dosages of 875 g/t, 1000 g/t, and 1125 g/t. The microscopic images clearly show that at lower CPAM dosages, the flocs formed during flocculation and sedimentation are smaller, mostly below 5 μm, resulting in a slower settling velocity. As the CPAM dosage increases, the size of the flocs increases, and the number of floc particles rises, consistent with the laser particle size analysis results. At a dosage of 1000 g/t, the floc size generally reaches about 10 μm, and the flocs remain as discrete entities. When the dosage is increased to 1125 g/t, the floc size exceeds 15 μm. Excessive hydrophilic CPAM leads to increased water entrapment within the flocs, a decrease in floc density, and an increase in the viscosity of the sedimentation system due to the surplus polymer, ultimately causing a decline in floc settling velocity. The floc morphology analysis indicates that 1000 g/t CPAM is the optimal dosage for the flocculation and sedimentation of fine-grained phosphate tailings slurry. Exceeding this dosage will impede the sedimentation process.

3.5. Dynamic Analysis of Particle Size and Morphology

Figure 13 presents the PVM test results of the phosphate tailings slurry before and after the addition of 1000 g/t CPAM (MW: 12 million). As illustrated, over time, the floc size distribution remains within the 10–100 μm counting range, irrespective of reagent addition. Compared to the untreated slurry, the introduction of CPAM significantly enhances the floc size of phosphate ore particles. Specifically, the average floc size of the untreated slurry decreases at the 2 min mark and subsequently stabilizes around 35 μm. In contrast, for the CPAM-treated slurry, the average floc size exhibits an initial increase followed by a decrease during the 2–8 min interval, eventually stabilizing near 53 μm. Analysis of the unweighted chord length distribution reveals that as time progresses from 5 to 11 min, the particle floc size distribution shifts to the right in both cases. This shift indicates a gradual reduction in smaller flocs and a corresponding increase in larger flocs. In the untreated slurry, this phenomenon is attributed to spontaneous aggregation, whereas in the CPAM-treated slurry, it results from floc bridging and adsorption mechanisms. Conversely, in the CPAM-treated slurry, flocs appear relatively dispersed at 2 min, progressively evolving toward a more

aggregated state, and ultimately reaching a substantially stable floc aggregate structure by 11 min.

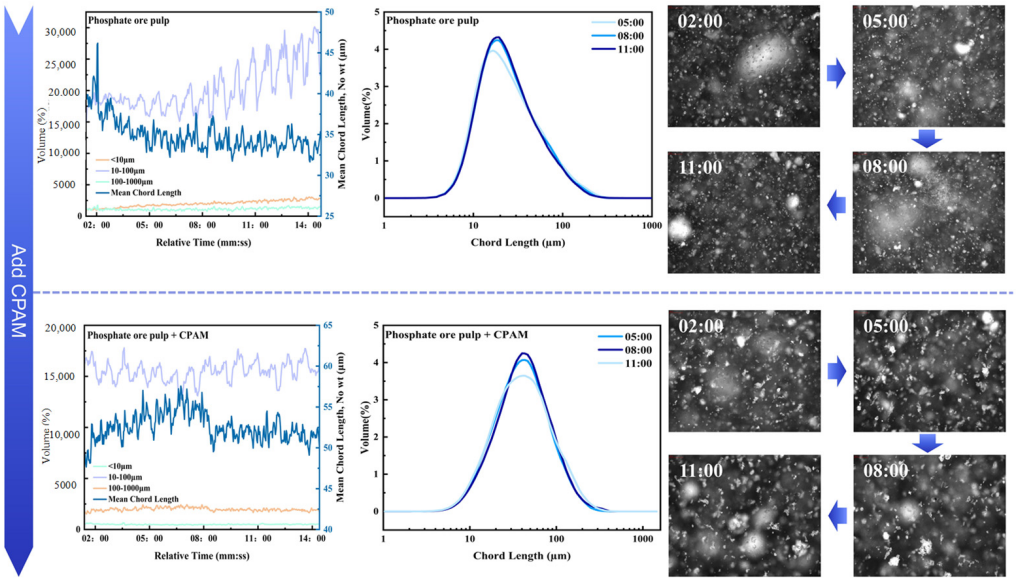


Figure 13. Dynamic particle size analysis of phosphate tailings slurries before and after adding 1000 g/t CPAM (MW: 12 million) by PVM.

3.6. Zeta Potential Analysis

The variation in mineral surface potential can directly reflect the adsorption behavior of reagents [27,28]. Zeta potential measurements of the phosphate tailings slurry were conducted before and after the addition of CPAM (MW: 12 million), with the reagent dosage set at 1000 g/t, as shown in Figure 14a. As illustrated, the isoelectric point of the phosphate tailings slurry sample occurs near pH 2.2, and the overall potential is negative, which is generally consistent with previous studies [29–31]. Upon the addition of CPAM, the slurry potential increases significantly. The maximum difference in potential before and after reagent addition, approximately 31.5 mV, is observed within the pH range of 3–5, indicating the strongest adsorption capacity of CPAM on the surface of phosphate tailings slurry particles under these conditions. As the pH continues to rise, the potential difference between the treated and untreated slurry gradually decreases. The CPAM molecular chain contains a large number of cationic groups. The ionization of these cationic groups in water imparts a strong positive charge to the CPAM polymer chain, promoting electrostatic neutralization on the negatively charged surfaces of phosphate tailings slurry particles. This process disrupts the stability of the colloidal system, allowing fine particles to approach each other and undergo flocculation.

To establish the quantitative correlation between Zeta potential shifts and floc size evolution, the test data from the laser particle size analyzer and Zeta potential meter were integrated to plot the correlation scatter diagram and temporal variation curve. The results showed a significant positive correlation between Zeta potential and floc D_{50} (R^2 = 0.80). The Zeta potential of the pulp increased rapidly from −5.307 mV to −2.85 mV within 0~3 min under the action of CPAM, which created conditions for the rapid growth of floc size in the subsequent 3~8 min. Figure 14b shows that when the Zeta potential increased from −5.307 mV to the range of −8.07~−2.39 mV, the floc D50 increased by 115% synchronously with a correlation coefficient of R^2 = 0.89, indicating that the potential rise caused by electrostatic neutralization is the key driving factor for the increase in floc particle size. It was confirmed that electrostatic neutralization reduced the inter-particle

repulsion and provided a necessary prerequisite for polymer bridging flocculation, with a clear temporal and quantitative correlation between them.

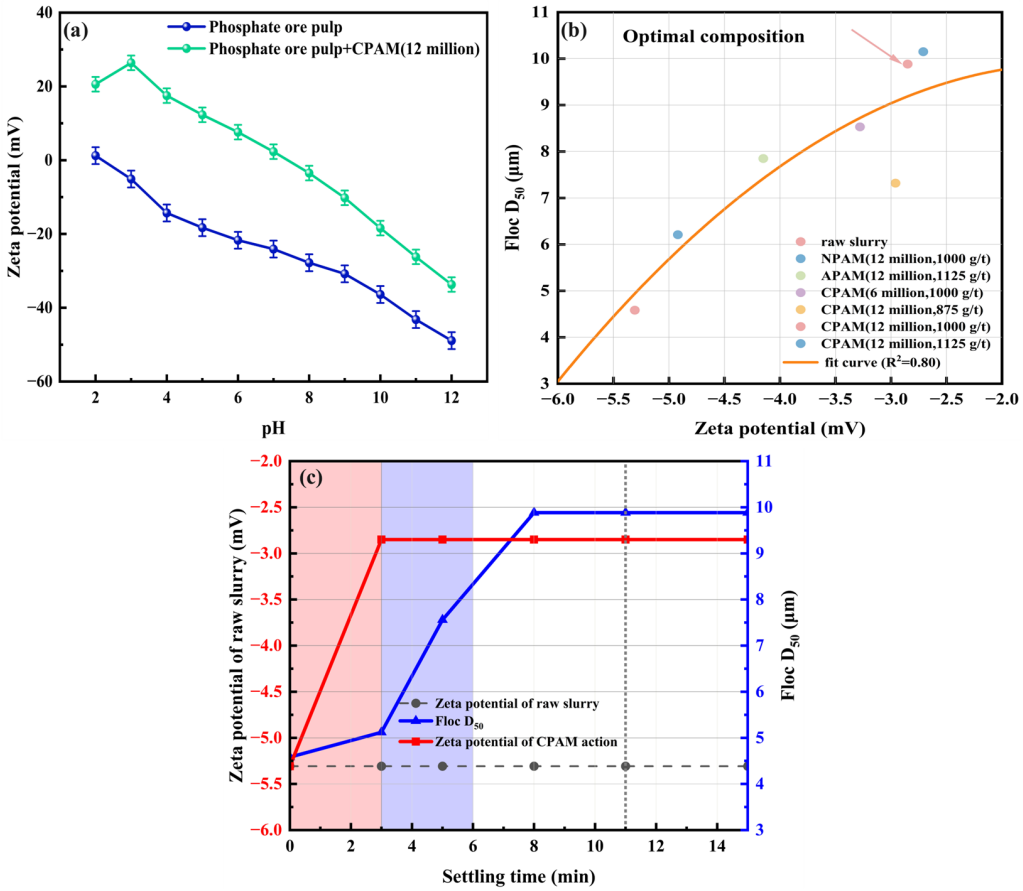


Figure 14. (**a**) Zeta potential variation in phosphate tailings slurries with pH value before and after adding 1000 g/t CPAM (MW: 12 million). (**b**) The sequential changes in Zeta potential and floc D50 under the action of CPAM (12 million,1000 g/t). (**c**) Correlation between Zeta potential and floc D50 under different PAM conditions.

3.7. FTIR Analysis

The infrared spectra of the phosphate ore before and after interaction with the flocculant are displayed in Figure 15. The spectral lines show the transmission infrared spectrum of phosphate ore. The absorption peaks at 1096 and 1043 cm^{-1} are attributed to the antisymmetric stretching vibration peak of PO_4^{3-}. The absorption peaks at 604 and 570 cm^{-1} correspond to the antisymmetric bending vibration of PO_4^{3-}. The absorption peaks at 1456 and 1430 cm^{-1} are attributed to the CO_3^{2-} antisymmetric stretching vibration peak. It is generally believed that CO_3^{2-} ions mainly enter the apatite lattice in a homomorphic substitution manner, forming fluorocarbon apatite.

There are residual substances in the previous process. Phosphate ore contains amide groups. After the heating treatment, the infrared test is conducted. For the phosphate ore adsorbing polyacrylamide, the intensities of the characteristic peaks of the amide groups at 1622 cm^{-1} were enhanced. The peak intensity of the characteristic peak of C-N at 1120 cm^{-1} slightly increased. The intensity of the free $-NH_2$ peak (at 3440 cm^{-1}) slightly increased. These changes indicate that polyacrylamide is adsorbed onto the surface of phosphate ore.

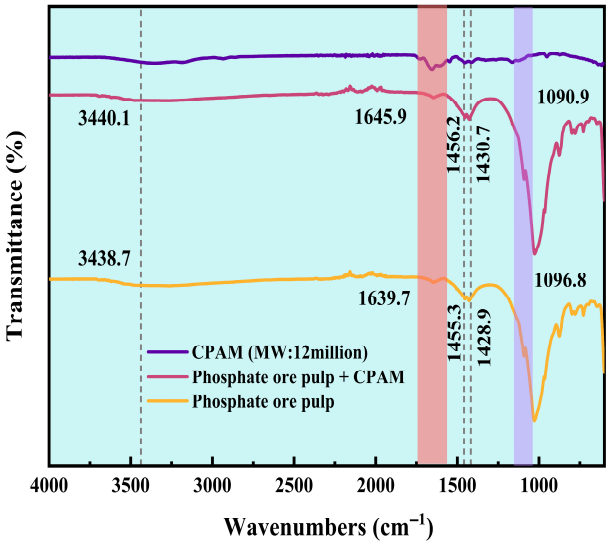


Figure 15. FTIR transmission spectra of phosphate tailings slurries before and after adding 1000 g/t CPAM (MW: 12 million).

4. Discussion

4.1. An Analysis of Flocculation Process

Based on the phenomenon of flocculation and sedimentation experiments, the sedimentation process of floc particles is divided into four stages.

As shown in Figure 16a, A-A represents the clear liquid level. After settlement begins, the relative velocity between floc particles and water gradually increases under downward acceleration. As shown in Figure 16b, B-B represents the sedimentation liquid level. As the relative velocity between floc particles and water increases, the drag force on floc particles during sedimentation also gradually increases. Then, the settling layer begins to form as the floc particle group gradually settles downwards. As shown in Figure 16d, the sedimentation liquid level in the measuring cylinder coincides with the clarification liquid level. Under the action of gravity, the sedimentation of "particles" continues, continuously rearranges the flocs and squeezes out the free water trapped within the network. Due to the low water content, the turbulent disturbance caused by the flow of rising water is weakened, and the drainage process tends to be slow. By relying solely on the gravitational force of flocs to expel water, the settling velocity is significantly reduced.

Compaction Settling Stage:

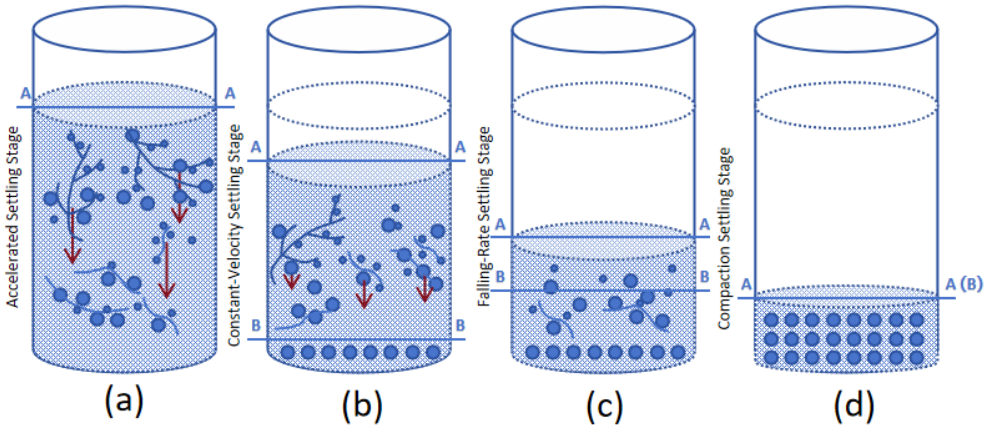


Figure 16. Schematic diagram of the four stages of floc particle sedimentation in phosphate tailings slurries ((**a**): accelerated settling, (**b**): constant-velocity settling, (**c**): falling-rate settling, (**d**): compaction settling).

4.2. The Bridging Mechanism of Flocculants in Phosphate Ore Particles

As shown in Figure 17, upon adding PAM to the slurry, one segment (or terminal group) of the polymer chain first adsorbs onto the mineral particle surface, with the remaining long polymer chain extending outward into the aqueous solution. The molecules can adsorb onto other particles through collision and contact, thereby forming a bridging effect. Known as unstable particles, they produce flocs. Many non-ionic polyacrylamide molecules on unstable particles adsorb onto another particle with adsorption vacancies. Random flocs are formed through the bridging effect. At this point, non-ionic polyacrylamide molecules play a bridging role between two particles, forming irregular flocs.

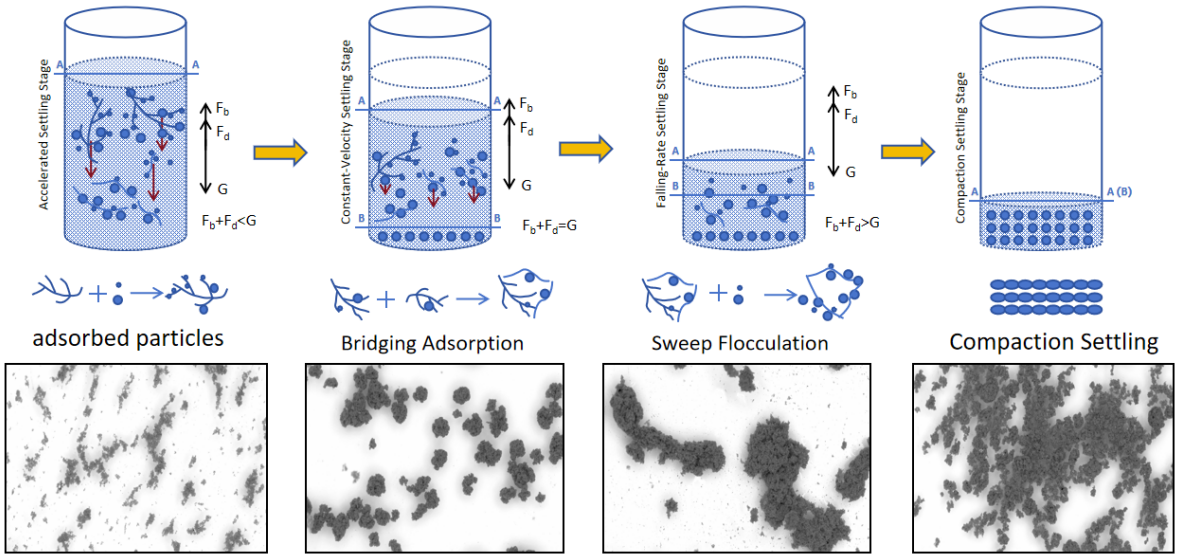


Figure 17. Schematic diagram of sedimentation process and flocculation bridging mechanism of phosphate tailings slurry particles treated with polyacrylamide flocculant.

The segment of the non-ionic polyacrylamide molecule that extends towards the solution from unstable particles may, due to the polymer's linear structure and abundant functional groups, entangle with and re-adsorb onto its own particle surface during movement [32–36]. This self-adsorption effectively covers the particle surface, locally inducing a dispersing effect (or steric hindrance) that prevents the polymer from forming a stable bridging effect with other particles. The resulting loose flocs, formed through limited bridging, undergo mechanical dehydration shrinkage when subjected to external forces, compressing the irregular structure into denser floc agglomerates.

It should be noted that if excessive amounts of polyacrylamide are used, the surface of each particle will be saturated with polyacrylamide molecules and there will be no more adsorption vacancies [37–40]. Polyacrylamide can no longer achieve bridging effect, but it instead stabilizes the dispersed system due to the steric hindrance effect. If the flocs formed by bridging action continue to be stirred vigorously or for a long time, the flocs will be dispersed and broken, forming scattered flocs. During the movement of the dispersed flocs, they undergo secondary adsorption by the polymer carried by the particles themselves, forming stable dispersed flocs again. Due to its dispersing effect, the dispersed system forms a stable protective colloid, making it less prone to flocculation. Therefore, to minimize significant experimental errors, the flocs must be sampled immediately after the coagulation and sedimentation experiment is completed and protected before any subsequent research or dewatering tests.

PAM molecules can adsorb onto the surface of phosphate ore particles through hydrogen bonding and electrostatic interactions, thereby forming inter-particle "bridges"

to agglomerate fine particles [41–43]. In the experimental system, the dosage of PAM is moderate (the dosage of CPAM with a molecular weight of 12 million is 1000 g/t), which avoids excessive overlap of molecular chains. Meanwhile, the linear structure of PAM enables it to fully extend and connect adjacent particles, thus confirming that bridging flocculation dominates in this experiment.

4.3. Cost and Benefit Analysis

As shown in Table 2, the dosage of PAM is extremely low in phosphate ore dehydration. Specifically, in this paper, when prepared at a concentration of 0.5% (five per thousand), the chemical consumption per ton of phosphate ore tailings is only about 1 kg. The industrial price of commonly used PAM ranges from 10 to 50 yuan per kilogram, while the reference price of phosphate concentrate with a grade of 30% is approximately ¥1050 to 1150 per ton. From the perspective of cost and benefit, it is reasonable to use the organic flocculant polyacrylamide as the dehydration agent for phosphate ore tailings.

Table 2. Cost accounting of PAM agent usage.

Economic Indicators	Value Range (CNY/ton of Fluorapatite)
Dehydration Agent Cost (PAM)	10–50
Revenue from Corresponding Phosphate Concentrate	315–345
Theoretical Profit (Before Deducting Other Production Costs)	265–335

Detailed Calculation Bases

(1) Dehydration Agent Cost Calculation

The PAM flocculant is configured at a concentration of 0.5% (five per thousand) for practical application in phosphate tailings slurry dehydration. According to industrial production experience, the dosage of PAM per ton of phosphate tailings slurry is approximately 1 kg. Considering the price range of industrially commonly used PAM products (which varies slightly by purity, molecular weight, and application scenario), the unit price of PAM is set at 10–50 CNY/kg. Thus, the dehydration agent cost per ton of fluorapatite is derived from the product of PAM dosage per ton and its unit price (1 kg/ton × 10–50 CNY/kg).

(2) Concentrate Revenue Calculation

For the purpose of intuitive economic comparison, this analysis assumes a 100% mineral processing recovery rate of phosphate tailings slurry (note: this is an idealized assumption for cost–benefit reference only; the actual recovery rate needs to be adjusted according to specific processing technology and equipment conditions). The reference price of phosphate concentrate with a grade of 30% (a common industrial grade) is 1050–1150 CNY/ton. The revenue from the concentrate corresponding to each ton of fluorapatite is calculated by multiplying the tailing quantity, grade conversion factor, and concentrate unit price (1 ton of tailings × 30% × 1050–1150 CNY/ton of concentrate).

(3) Theoretical Profit Calculation

The theoretical profit per ton of fluorapatite is obtained by subtracting the dehydration agent cost from the concentrate revenue. It is important to emphasize that this profit value is a preliminary theoretical result, as it does not include other production costs such as energy consumption during mineral processing, equipment wear and tear, labor costs, and transportation expenses. However, even when considering these additional costs, the extremely low proportion of PAM agent cost (accounting for only 3.2–15.9% of the concentrate revenue) ensures a significant profit margin for industrial production.

5. Conclusions

(1) The phosphate tailings slurry from a phosphate mine in Yichang primarily consists of dolomite and gypsum, with minor amounts of fluorapatite, hydroxyapatite, quartz, and other minerals. Its particle size distribution was characterized using a laser particle size analyzer. The content of fine particles in phosphate tailings is very high, and the content of coarse particles is relatively low, belonging to ultrafine slurry. Therefore, the phosphate tailings slurry of the phosphate plant is difficult to settle.

(2) Sedimentation experiments were conducted using flocculants of different molecular weights. The experimental results show that the sedimentation effect of high-molecular-weight flocculants is better than that of low-molecular-weight flocculants. High-molecular-weight flocculants exhibit superior sweep flocculation efficiency, enabling them to entrap more small-sized flocs and form larger, denser floc aggregates.

(3) The sedimentation and dehydration experiments of three different types of flocculants showed that the Zeta potential of the phosphate tailings slurry was negative. The coagulation and sedimentation effect of CPAM is best under the action of electric neutralization. At the same time, under the action of CPAM, the dewatering effect of phosphate tailings slurry is also the best. CPAM is the most effective flocculant in the experiment.

(4) The settling behavior of phosphate tailings particles was analyzed, and the settling process was divided into four stages: acceleration stage, constant velocity stage, deceleration stage, and floc compaction stage. Furthermore, the bridging flocculation theory was employed to elucidate the action mechanism of flocculants on phosphate tailings particles, yielding certain theoretical value for the solid–liquid separation process in fluorapatite beneficiation.

Author Contributions: Conceptualization, F.L., Y.F. (Yuping Fan) and W.X.; Methodology, F.L., Y.F. (Yuping Fan) and Y.F. (Yuanpeng Fu); Software, F.L.; Validation, X.M. and W.F.; Data curation, W.X. and W.F.; Writing—original draft, F.L. and Y.Z.; Writing—review & editing, F.L.; Visualization, F.L. and Y.F. (Yuanpeng Fu); Supervision, X.D.; Project administration, X.D.; Funding acquisition, Y.Z. All authors have read and agreed to the published version of the manuscript.

Funding: This study is supported by the Fundamental Research Program of Shanxi Province (202403021221068, 202403021211070). This work was also supported by the National Natural Science Foundation of China (No. 52504303). This study is supported by the China Postdoctoral Science Foundation (2025M781730).

Data Availability Statement: Data is contained within the article.

Conflicts of Interest: The authors declare no conflict of interest. Author Fang Li was employed by the company Hubei Xingfa Chemical Group Co., Ltd., Yichang 443311, China. The remaining authors declare that the research was conducted in the absence of any commercial or financial relationships that could be construed as a potential conflict of interest. Author Yangge Zhu was employed by the company, State Key Laboratory of Mineral Processing, BGRIMM Technology Group, Beijing 100044, China. The remaining authors declare that the research was conducted in the absence of any commercial or financial relationships that could be construed as a potential conflict of interest.

References

1. Cordell, D.; Drangert, J.-O.; White, S. The story of phosphorus: Global food security and food for thought. *Glob. Environ. Change* **2009**, *19*, 292–305. [CrossRef]
2. de Freitas Simões, F.; Borges, J.P.; Pires, N.J.; dos Santos Oliveira, M. High-intensity magnetic separation as a pre-flotation stage for the purification of complex phosphate ore. *Sep. Purif. Technol.* **2025**, *378*, 134704. [CrossRef]
3. He, D.; Shen, H.; Fu, Y.; Chen, F.; Li, Z.; Tang, Y.; Chen, Y.; Hassan, E.-S.R. Double reverse flotation of low-grade high-potassium phosphate ores: Selective separation of dolomite and potassium feldspar via targeted reagent interactions. *Appl. Surf. Sci.* **2026**, *715*, 164476. [CrossRef]

4. Lan, S.; Dong, L.; Shen, P.; Zhang, T.; Liu, D.; Shen, Z. An eco-friendly depressant to achieve efficient and clean reverse flotation enrichment of phosphate ores. *Appl. Surf. Sci.* **2025**, *713*, 164249. [CrossRef]
5. Ou-Douaou, A.; Akhtach, S.; Oulkhir, A.; Benhida, R.; Danouche, M. Advances in microbial biosurfactants for mineral flotation: Towards sustainable phosphate ore beneficiation. *J. Water Process Eng.* **2025**, *76*, 108267. [CrossRef]
6. Zhang, Y.; Yan, Y.; Yang, B.; Ma, R.; Xu, Y.; Luo, H.; Zhou, F. The efficient removal of dolomite from phosphate ores using a novel collector: Flotation selectivity and collecting mechanism. *Miner. Eng.* **2025**, *234*, 109768. [CrossRef]
7. Bergani, A.; Taha, Y.; Ait-Khouia, Y.; Hakkou, R.; Benzaazoua, M. Enhancing flocculation and dewatering performance of fine phosphate tailings: A sustainable approach for water resources management. *Sep. Purif. Technol.* **2025**, *359*, 130377. [CrossRef]
8. Ettoumi, M.; Jouini, M.; El-Bahi, A.; Bergani, A.; Taha, Y.; Khalil, A.; Benzaazoua, M. Extraction and application of flaxseed-derived bioflocculants for phosphate tailings densification. *J. Water Process Eng.* **2025**, *75*, 108001. [CrossRef]
9. Reid, C.; Bécaert, V.; Aubertin, M.; Rosenbaum, R.K.; Deschênes, L. Life cycle assessment of mine tailings management in Canada. *J. Clean. Prod.* **2009**, *17*, 471–479. [CrossRef]
10. Bergani, A.; Ait-Khouia, Y.; El-Bahi, A.; Hakkou, R.; Benzaazoua, M.; Taha, Y. Advancing sustainable dewatering of fine phosphate tailings: Evaluating xanthan gum, sodium alginate, and carboxymethyl cellulose as flocculating agents. *Water Res.* **2025**, *280*, 123526. [CrossRef]
11. Choumane, F.Z.; Benguella, B.; Maachou, B.; Saadi, N. Valorisation of a bioflocculant and hydroxyapatites as coagulation-flocculation adjuvants in wastewater treatment of the steppe in the wilaya of Saida (Algeria). *Ecol. Eng.* **2017**, *107*, 152–159. [CrossRef]
12. Renault, F.; Sancey, B.; Charles, J.; Morin-Crini, N.; Badot, P.-M.; Winterton, P.; Crini, G. Chitosan flocculation of cardboard-mill secondary biological wastewater. *Chem. Eng. J.* **2009**, *155*, 775–783. [CrossRef]
13. Kadooka, H.; Kiso, Y.; Goto, S.; Tanaka, T.; Jami, M.S.; Iwata, M. Flocculation behavior of colloidal suspension by use of inorganic and polymer flocculants in powder form. *J. Water Process Eng.* **2017**, *18*, 169–175. [CrossRef]
14. Suparmaniam, U.; Lam, M.K.; Uemura, Y.; Shuit, S.H.; Lim, J.W.; Show, P.L.; Lee, K.T.; Matsumura, Y.; Le, P.T.K. Flocculation of Chlorella vulgaris by shell waste-derived bioflocculants for biodiesel production: Process optimization, characterization and kinetic studies. *Sci. Total Environ.* **2020**, *702*, 134995. [CrossRef]
15. Molaei, N.; Chelgani, S.C.; Bobicki, E.R. A comparison study between bioflocculants and PAM for dewatering of ultrafine phyllosilicate clay minerals. *Appl. Clay Sci.* **2022**, *218*, 106409. [CrossRef]
16. Zhang, H.; Guan, G.; Lou, T.; Wang, X. High performance, cost-effective and ecofriendly flocculant synthesized by grafting carboxymethyl cellulose and alginate with itaconic acid. *Int. J. Biol. Macromol.* **2023**, *231*, 123305. [CrossRef]
17. Yue, Y.; Zheng, L.; Wang, Y.; Wu, J.; Li, S.; Han, X.; Wu, L. A novel polyamidine-grafted carboxymethylcellulose: Synthesis, characterization and flocculation performance test. *e-Polymers* **2019**, *19*, 225–234. [CrossRef]
18. Hamraoui, L.; Bergani, A.; Ettoumi, M.; Aboulaich, A.; Taha, Y.; Khalil, A.; Neculita, C.M.; Benzaazoua, M. Towards a Circular Economy in the Mining Industry: Possible Solutions for Water Recovery through Advanced Mineral Tailings Dewatering. *Minerals* **2024**, *14*, 319. [CrossRef]
19. Moud, A.A. Polymer based flocculants: Review of water purification applications. *J. Water Process Eng.* **2022**, *48*, 102938. [CrossRef]
20. Ren, B.; Xu, M.; Huang, X.; Zhu, J.; Liu, C.; Min, F. Influence of polyacrylamide-based flocculant dosing sequence on the flocculation bridging mechanism of kaolinite: Experimental and MD simulation insights. *Surf. Interfaces* **2026**, *83*, 108528. [CrossRef]
21. Wang, J.; Wang, Y.; Ma, T.; Xu, G.; Feng, M. Synergistic mechanism of adsorption-diffusion at quartz-water interface for the dewatering of waste slurry using APAM flocculant: Insights from molecular dynamics simulation. *J. Water Process Eng.* **2023**, *55*, 104275. [CrossRef]
22. Loukili, N.; Jossic, L.; Blésès, D.; Oliveira, M.; Fayolle, Y.; Ginisty, P.; Elkissi, N.; Magnin, A.; Rharbi, Y. Impact of cationic polyacrylamide degradation on flocculation in wastewater treatment. *Colloids Surf. A Physicochem. Eng. Asp.* **2024**, *702*, 134975. [CrossRef]
23. Cheng, D.; Ao, X.; Yuan, X.; Liu, Q. Effect of dissolved metal ions from mineral surfaces on the surface wettability of phosphate ore by flotation. *Colloids Surf. A Physicochem. Eng. Asp.* **2024**, *701*, 134995. [CrossRef]
24. Liu, X.; Li, C.; Luo, H.; Cheng, R.; Liu, F. Selective reverse flotation of apatite from dolomite in collophanite ore using saponified gutter oil fatty acid as a collector. *Int. J. Miner. Process.* **2017**, *165*, 20–27. [CrossRef]
25. Zeng, L.; Ding, K.; Zhang, X.; Zhou, Y.; Han, H. New insights into the influence of mineral surface transformation on the flotation behavior of anhydrite/apatite. *Colloids Surf. A Physicochem. Eng. Asp.* **2024**, *685*, 133215. [CrossRef]
26. Vučinić, D.R.; Radulović, D.S.; Deušić, S.Đ. Electrokinetic properties of hydroxyapatite under flotation conditions. *J. Colloid Interface Sci.* **2010**, *343*, 239–245. [CrossRef]

27. Oulkhir, A.; Lyamlouli, K.; Oussfan, A.; Orange, F.; Etahiri, A.; Benhida, R. Efficient flotation separation approach of apatite from calcite for phosphate up-grading using phosphorylated starch macromolecules as a selective depressant. *Carbohydr. Polym.* **2025**, *348*, 122878. [CrossRef] [PubMed]
28. Ma, R.; Yang, B.; Deng, B.; Shao, H.; Xiao, Y.; Luo, H. The efficient separation of apatite and dolomite using sodium dextran sulphate as an eco-friendly depressant: Flotation performances and atom-scale interaction mechanism. *Miner. Eng.* **2025**, *227*, 109291. [CrossRef]
29. Liu, C.; He, H.; Zhu, Y.; Xu, W.; Yang, S. The utilization of 1-Dodecyl-3-methylimidazolium bromine ionic liquid in the reverse flotation separation of feldspar from apatite. *Adv. Powder Technol.* **2024**, *35*, 104499. [CrossRef]
30. Liu, C.; Zhu, L.; Fu, W.; Chi, R.; Li, H.; Yang, S. Investigations of amino trimethylene phosphonic acid as a green and efficient depressant for the flotation separation of apatite from calcite. *Miner. Eng.* **2022**, *181*, 107552. [CrossRef]
31. Yu, H.; Zhu, Y.; Lu, L.; Hu, X.; Li, S. Removal of dolomite and potassium feldspar from apatite using simultaneous flotation with a mixed cationic-anionic collector. *Int. J. Min. Sci. Technol.* **2023**, *33*, 783–791. [CrossRef]
32. Wang, X.; Song, Q.; Xie, R.; Liu, J.; Zhu, Y. Selective flotation separation of scheelite from apatite by application of ATMP as an efficient depressant. *J. Mol. Liq.* **2023**, *378*, 121604. [CrossRef]
33. Wang, X.; Xie, R.; Liu, J.; Zhu, Y. The utilization of tamarind seed gum as a novel dolomite depressant in the selective flotation of apatite from dolomite. *Adv. Powder Technol.* **2023**, *34*, 104022. [CrossRef]
34. Xu, W.; Xu, X.; Xu, Z.; Guo, C.; Pan, W.; Mei, G. Selective flotation separation of apatite from quartz using an anionic combined collector: Co-adsorption behavior and mechanism. *Appl. Surf. Sci.* **2026**, *717*, 164815. [CrossRef]
35. Aarab, I.; El Amari, K.; He, D.; Fu, Y.; Boujounoui, K.; Etahiri, A. Eco-friendly apatite flotation: Unlocking the potential of spent coffee grounds as a bio-based collector. *Miner. Eng.* **2025**, *233*, 109652. [CrossRef]
36. He, K.; Zhang, D.; Wang, M.; Liu, R. Efficient magnesium removal by reverse flotation of apatite using cyclic modified fatty acid soaps: Experiment and DFT calculation. *Miner. Eng.* **2026**, *235*, 109804. [CrossRef]
37. Zhang, C.; Liu, P.; Zhang, W.; Dai, H.; Tian, Y.; Tian, M.; Sun, W. Study on the adsorption selectivity of a novel fatty acid collector on apatite, dolomite, and calcite surfaces for improved flotation. *Miner. Eng.* **2025**, *232*, 109523. [CrossRef]
38. Zhong, C.; Feng, B.; Zhang, L.; Zhang, W.; Wang, H.; Gao, Z. Flotation separation of apatite and calcite using gum arabic as a depressant. *Colloids Surf. A Physicochem. Eng. Asp.* **2022**, *632*, 127723. [CrossRef]
39. Chang, S.; Zhang, J.; Liu, Z.; Gao, K.; Zhang, D.; Huang, J. Activation mechanisms of apatite by purifying reagent polyacrylamide for backwater from mineral processing in flotation of rare earths. *Adv. Powder Technol.* **2021**, *32*, 4447–4460. [CrossRef]
40. Bazoubandi, B.; Soares, J.B. Amylopectin-graft-polyacrylamide for the flocculation and dewatering of oil sands tailings. *Miner. Eng.* **2020**, *148*, 106196. [CrossRef]
41. Mu, Y.; Ma, X.; Fan, Y.; Dong, X.; Zhang, C.; Li, N.; Fang, W. A comparative study of the effects of industrial water and ultrapure water on the sedimentation and dewatering performance of fine coal tailings. *Int. J. Coal Prep. Util.* **2025**, 1–19. [CrossRef]
42. Li, N.; Fan, Y.; Dong, X.; Ma, X.; Chen, R.; Chang, M.; Xu, G. Synthesis and characterization of a guar gum-based flocculant and its flocculation-dewatering mechanism in coal mine wastewater. *Int. J. Biol. Macromol.* **2025**, *308*, 142438. [CrossRef] [PubMed]
43. Fan, Y.; Ruan, C.; Chang, M.; Dong, X.; Ma, X.; Ye, G. Effect of settling vortex of coal slime flocs with different sizes on the settlement of microfine particles. *Powder Technol.* **2025**, *452*, 120422. [CrossRef]

Disclaimer/Publisher's Note: The statements, opinions and data contained in all publications are solely those of the individual author(s) and contributor(s) and not of MDPI and/or the editor(s). MDPI and/or the editor(s) disclaim responsibility for any injury to people or property resulting from any ideas, methods, instructions or products referred to in the content.